Thin Solid Films 825 (2025) 140740

Contents lists available at ScienceDirect

Thin Solid Films

journal homepage: www.elsevier.com/locate/tsf

Antibacterial efficacy of ultrafast laser-induced periodic structures on SUS304 surfaces with Ag and Cu coatings

Jyun-Jhih Wang [a,*], Ya-Zhen Xu [b], Chun-Ming Chen [a], Yu-Chung Lin [a], Chien-Jung Huang [a], Ying-Hong Lin [b], Hsuan-Kai Lin [c,*]

[a] Department of Laser Micro-processing Technology, Industrial Technology Research Institute Southern Region Campus, Tainan, Taiwan
[b] Department of Plant Medicine, National Pingtung University of Science and Technology, Pingtung, Taiwan
[c] Department of Materials Engineering, National Pingtung University of Science and Technology, Pingtung, Taiwan

ARTICLE INFO

Keywords:
Laser-induced periodic surface structures (LIPSSs)
Picosecond laser
Surface modification
Antibacterial properties

ABSTRACT

SUS304 substrates are processed using a picosecond UV laser at various laser fluences to produce laser-induced periodic surface structures (LIPSSs). Thin Ag and Cu films with a thickness of 15 nm are deposited on both the original SUS304 substrate and the SUS304+LIPSS substrates. The morphologies, crystal structures, and element segregations of the SUS304 and SUS304+LIPSSs specimens are systematically examined and compared. The LIPSS period (Λ), surface wettability, surface roughness, and antibacterial properties of the various samples against *Escherichia coli, Staphylococcus aureus*, and *Pseudomonas aeruginosa* are also examined. No elemental segregation or phase transitions of the SUS304 surface are observed after picosecond UV laser irradiation. However, LIPSSs are observed at laser fluences of 6.63, 7.96, and 8.84 J/cm^2. The surface ripples on the SUS304+LPSS samples are perpendicular to the direction of the electric field (E) of the laser. The surface roughness (Ra), ripple period (Λ), and contact angle (CA) increase with increasing laser fluence. All of the coated samples show an antibacterial efficiency of 100 % against *E. coli, S. aureus*, and *P. aeruginosa* after 24 h. In addition, the SUS304+LIPSSs samples with Ag and Cu coatings limit the growth and proliferation of all three bacteria. The Ag-coated samples show a better ROS accumulation, and hence a greater cytotoxicity effect than the Cu-coated samples for all three bacteria. Overall, the results indicate that UV picosecond laser irradiation enables good control over the surface properties of the SUS304 substrate and has strong potential for enhancing the antibacterial performance and supporting further surface engineering improvements.

1. Introduction

Ultrafast lasers have a high peak power and ultrashort pulse duration and are widely used in precision micromachining and medical applications. Compared with conventional microsecond (ms) and nanosecond (ns) pulse laser modification techniques, ultrafast laser processing has the advantages of a smaller heat-affected zone (HAZ) [1], less contamination [2], higher reproducibility, and greater precision [3]. In addition, ultrafast lasers can effectively overcome the challenges posed by the oxide layers on high-strength alloys to create surfaces suitable for bioactive applications [4].

Laser-induced periodic surface structures (LIPSSs) consist of ripples caused by the self-alignment of the material when surface plasmon polaritons (SPPs) interact with ultra-fast laser pulses [1]. By adjusting the polarization direction [5] and spot size of the incident light [6], the uniformity and functionality of the LIPSSs can be tuned for many applications in the fields of biomedicine and materials science. LIPSSs possess strong antireflection, wettability, biocompatibility, and antifriction properties [7–9]. LIPSS is used to cover numerous solid materials and is widely used in many fields, including biomedicine [9] and environment [10]. Furthermore, LIPSSs significantly reduce surface adhesion [11]. LIPSSs provide a controllable method for achieving nanoscale structures with a wide variety of properties and have thus attracted considerable attention in the literature [12,13]. One potential application of LIPSS is to increase the antibacterial activity of materials used in biomedical applications, such as implants and surgical instruments. Many previous studies have demonstrated the excellent antimicrobial effects of thin films and metal nanoparticles against fungi (*Colletotrichum gloeosporioides*) [14] and bacteria (*E. coli, Staphylococcus aureus*, and *Pseudomonas aeruginosa*) [15–18]. However, the literature

* Corresponding authors.
E-mail addresses: JJWang0323@itri.org.tw (J.-J. Wang), HKLin@mail.npust.edu.tw (H.-K. Lin).

https://doi.org/10.1016/j.tsf.2025.140740
Received 13 February 2025; Received in revised form 1 July 2025; Accepted 3 July 2025
Available online 4 July 2025

contains scant information on the combination of LIPSS formation and thin-film deposition as a strategy for enhancing antibacterial effects. Accordingly, the present study applies a picosecond UV laser to produce periodic LIPSS nanostructures on SUS304 substrates. Thin Ag and Cu films with a thickness of 15 nm are then deposited on the LIPSS structures to form antibacterial coatings. The morphologies, crystal structures, and element segregations of the SUS304 and SUS304+LIPSSs specimens are examined and compared. In addition, the antimicrobial efficacies of the various samples are evaluated using three common bacterial strains: *E. coli, S. aureus,* and *P. aeruginosa* efficacy. Overall, the results show that UV picosecond laser irradiation enables good control over the surface properties of the SUS304 substrate and, in combination with thin film deposition, has a strong potential for enhancing the antibacterial performance of common biomedical substrate materials.

2. Materials and methods

Polished SUS304 disks were purchased from Yuan-Yi Co. Ltd., Taiwan. The disks were cleaned sequentially in acetone, ethanol, and deionized water for 10 min and then air-dried. LIPSSs were formed on the SUS304 surface using a picosecond laser (TruMicro 5370, TRUMPF, Germany) with a wavelength of 343 nm, pulse duration of 5 ps, repetition rate of 400 kHz, and maximum power of 30 W. The output beam was collimated by a beam expander to produce a beam diameter of 2.5 mm which the definition is according to the 1/e (36.8 %) and beam quality (M^2) of 1.09. The laser beam was delivered to the surface of the SUS304 disks using a scanning galvanometer and f-theta lens with the focal length of 80 mm. The laser was operated at a constant scan speed and repetition rate of 1000 mm/s and 400 kHz, respectively, with powers of 0.8, 1.5, 1.8, and 2.0 W. The corresponding fluences of the laser were evaluated as

$$\text{Fluence } (\text{J}/\text{cm2}) = \frac{\frac{P}{f}}{\pi r^2} \quad (1)$$

where P is the laser power (W), f is the repetition rate (Hz), and r is the laser spot radius (12 μm). The fluence values were thus 3.54, 6.63, 7.96, and 8.84 J/cm^2, respectively.

Laser processing was conducted over an area of 20 mm × 20 mm. Following laser treatment, the disks were washed with alcohol in an ultrasonic bath for 10 min and then air dried. Ag and Cu thin films with a thickness of 15 nm were deposited on the SUS304 disks with and without nanostructures using a high-vacuum sputtering system (KD-SPUTTER+LL, Kao Duen Co., Ltd., Taiwan). Prior to the sputtering deposition, the vacuum chamber was evacuated to a base pressure lower than 2.67×10^{-4} Pa to minimize contamination. High-purity argon (Ar) gas was introduced at a controlled flow rate of 30 standard cubic centimeters per minute (sccm), establishing a stable working pressure of 6.67×10^{-1} Pa during deposition. Cu and Ag thin films were deposited by magnetron sputtering using 99.99 % pure metallic targets (diameter: 50.8 mm). The Cu film was performed at a sputtering power of 42 W for 49 s and Ag film was performed 45 W for 45 s under identical chamber conditions. These conditions were maintained to ensure consistent film quality and reproducibility across all samples. The surface morphologies and elemental compositions of the various samples were observed using a field-emission scanning electron microscope equipped with an energy-dispersive X-ray spectrometer (EDS, FE-SEM, JEOL, JSM-7600 F, Japan) with a working voltage of 15 kV. The crystal structures of the samples were examined using X-ray diffraction (XRD, Bruker, D8, USA) with an incident wavelength of $\lambda = 0.154$ nm, incident angle of 1 degree and the operating voltage, current of 40 kV and 40 mA, respectively. The wettability of the samples was measured by a contact angle system (OCA 15EC, Germany) using 1-μl distilled water droplets placed at five different locations on the sample surface. After LIPSS formation, the contact angle was measured after one day. Finally, the surface roughness (Ra) of the samples was measured using a surface roughness analyzer with the precision of depth direction of nanometers to 1200 μm (Alpha-Step, KLA, d-300, USA) under a load of 15 mg. To ensure the reliability and repeatability of the measurement results, the surface roughness was measured at five different locations on the sample surface.

E. coli (ATCC23815), *S. aureus*, and *P. aeruginosa* bacteria strains were cultured in lysogeny broth (LB) at 37 °C and agitated at 150 rpm for 8 h. The strains were then deposited on SUS304 and SUS304+LIPSS samples with and without Ag and Cu coatings at concentrations of 10^5 ml/colony-forming units (CFUs). The samples were incubated at 37 °C for 24 h under 100 % relative humidity (RH). The bacterial solutions were plated on nutrient agar (NA) and incubated at 37 °C for 8 h. Bacterial growth curves were constructed by sampling the suspensions every hour. The optical density (OD) of each sample was measured using a spectrophotometer (Spectrostar Nano, BMG LABTECH GmbH Co., Ltd, Germany) at a wavelength of 600 nm. The quantity of reactive oxygen species (ROS) and viability of the cells on the coated SUS304 and SUS304+LIPSS samples were evaluated after 24 h by staining with 20 μM H2DCFDA probe (Sigma, USA) and propidium iodide (PI; Sigma, USA) under dark conditions for 20 min. The stained samples were observed under a fluorescence microscope (Leica, Germany). For each sample, the quantity of ROS and the number of live and dead cells were evaluated using ImageJ software (National Institutes of Health, USA). In the ROS and PI assays, the live cells emitted green fluorescence, while the dead cells emitted red fluorescence. AlamarBlue assays were performed to quantitatively analyze the cell proliferation. Treated bacterial suspensions (90 μl) were mixed with alamarBlue reagent (Geno Technology, Inc., USA) (10 μl) and incubated for 30 min in a 96-well plate under dark conditions. The absorbance of the suspensions was then measured at 570 nm and 600 nm using a UV–visible spectrophotometer. The alamarBlue reduction rate (i.e., bacterial viability) of each sample was computed as

$$\text{Reduction of alamarBlue } (\%) = \frac{(\text{O2 x A1}) - (\text{O1 x A2})}{(\text{R1 x N2}) - (\text{R2 x N1})} \times 100 \quad (2)$$

where:

O1 = Molar Extinction Coefficient of OXIDIZED alamarBlue at 570 nm
O2 = Molar Extinction Coefficient of OXIDIZED alamarBlue at 600 nm
R1 = Molar Extinction Coefficient of REDUCED alamarBlue at 570 nm
R2 = Molar Extinction Coefficient of REDUCED alamarBlue at 600 nm
A1 = Absorbance value of test wells at 570 nm
A2 = Absorbance value of test wells at 600 nm
N1 = Absorbance value of Negative Control well at 570 nm
N2 = Absorbance value of Negative Control well at 600 nm

For descriptive statistics of normally distributed data sets, the results were expressed as mean ± standard error (SE) for all assays. One-way analysis of variance (ANOVA) was employed to assess statistical differences among groups. When a statistically significant difference was observed ($p < 0.05$), all pairwise multiple comparisons were conducted using Tukey's Honestly Significant Difference (HSD) test [19,20]. Each statistical analysis was based on three independent replicates. All statistical tests were performed using commercial software (SPSS V. 20, IBM).

3. Results and discussions

3.1. Effects of laser processing on surface morphologies and crystal structures of the SUS304

Fig. 1 shows the surface morphologies of the SUS304 substrates processed using various laser fluences. The original polished SUS304 specimen exhibits a smooth and highly uniform surface (Fig. 1(a)). However, following processing with a laser fluence of 3.54 J/cm^2, the surface develops a discontinuous stripe structure (Fig. 1(b)). As the laser fluence increases to 6.63, 7.96, and 8.84 J/cm^2, LIPSSs form on the sample surface, as shown in Fig. 1(c)–(e). The surfaces show a strong parallel-ripple characteristic, accompanied by dot-like nanoparticles between the ripples. For all the specimens, the ripples are oriented perpendicular to the direction of the electric field (E) of the laser.

LIPSSs typically form with fluences close to the ablation threshold of the material being necessary to produce uniform LIPSSs [1,21]. The spatial period and depth of LIPSSs are strongly dependent on the laser fluence and the number of pulses per processed area. However, these parameters are difficult to control independently [22]. The surface modulation depth of LIPSSs typically lies at the nanometer scale. This fine control over the surface modification pattern allows for the enhancement of various material properties, such as the wear resistance [23,24], corrosion resistance [24,25], and biomimetic characteristics [26]. The EDS results in Fig. 2(a) show that no element segregation occurs on the sample surfaces following picosecond laser irradiation. Table 1 presents the elemental compositions of the non-irradiated and laser-irradiated SUS304 specimens. The results show that the two samples have similar compositions. Furthermore, the XRD patterns in Fig. 2 (b) show three sharp peaks at 43°, 52° and 78°, indicating the single phases structure. The results also demonstrate that the irradiated sample maintains the same crystallization structure as the original sample. In other words, the picosecond laser treatment does not alter the primary crystallization properties of SUS304. This finding is reasonable since the picosecond laser produces only an extremely small heat-affected zone (HAZ) during processing, and the surface modification process thus occurs mainly through a multi-photon effect. Moreover, previous studies [1,24] have shown that the laser-affected depth in picosecond laser processing is approximately 30 μm, with the result that the surface layer undergoes only structural refinement rather than substantial transformation. However, the ultrafast laser irradiation process prompts a grain refinement effect, which creates structural dislocations on the sample surface that enhance both the mechanical properties of the material and the corrosion resistance [24].

3.2. Wettability and surface roughness of SUS304 specimens with LIPSSs

Fig. 3 illustrates the interrelationships among the laser fluence, LIPSS period, and surface roughness (Ra) of the processed SUS304 substrates. The surface roughness and LIPSS period both increase with increasing laser fluence. Specifically, the surface roughness increases from 30 nm (no laser treatment) to 62 nm (3.54 J/cm^2), 72 nm (6.63 J/cm^2), 78 nm (7.96 J/cm^2), and 96 nm (8.84 J/cm^2). As the laser fluence increases to 6.63 J/cm^2, LIPSSs are formed with a period of approximately 164 nm. As the laser fluence continues to increase, the ripple period increases slightly to 174 (7.96 J/cm^2) and 178 nm (8.84 J/cm^2). Moreover, the LIPSS interspace was usually evaluated by the distance between two neighbor structure. The inter space were 250, 256 and 258 nm, respectively. These results indicate that the laser fluence provides a viable means of fine-tuning the LIPSS period. Fig. 4 shows the contact angles of the water droplets placed on the original polished SUS304 substrate and the substrates processed with fluences of 3.54, 6.63, 7.96, and 8.84 J/cm, respectively. The original sample has a contact angle of 71.6° However, following laser irradiation, the contact angles increase to 111.6°, 115.6°, 114.1°, and 105.9°, respectively. In other words, the higher surface roughness produced by laser irradiation causes the surface of the SUS304 samples to become more hydrophobic [27]. Previous research has shown that the surface contact angle and surface energy are key factors determining the antibacterial effects of materials [15]. In addition, hydrophobic surfaces offer several other favorable characteristics such as self-cleaning [28], anti-corrosion [28], and anti-adherence [29]. Laser texturing provides a straightforward method for modifying the wettability of surfaces, thus opening up many potential applications.

The formation of nanostructures using picosecond laser pulses, as opposed to nanosecond laser pulses, is characterized by a shorter interaction time (pulse width) with the metal surface. This limited interaction time allows for more precise control over the nanostructure formation due to rapid vaporization and a very small HAZ [22]. In picosecond laser processing, high-energy laser photons are delivered to fine points for ablation, which enables the fabrication of structural

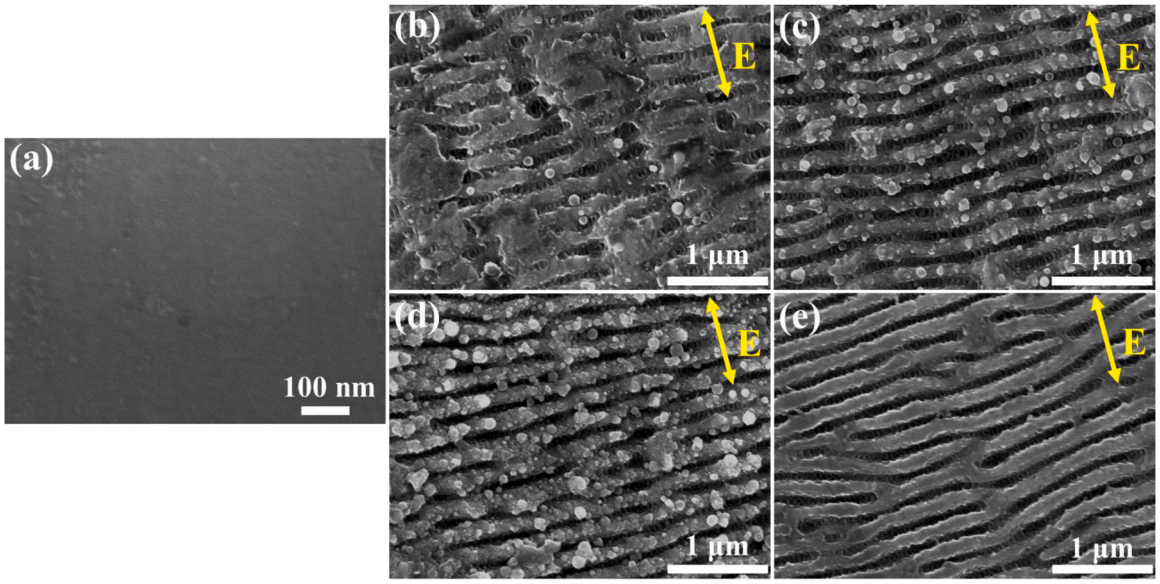

Fig. 1. SEM images of SUS304 substrates with LIPSSs produced using laser repetition rate of 400 kHz, scan speed of 1000 mm/s, and different fluences. (a) polished SUS304 surface with no nano-structures; SUS304 surfaces processed with laser fluences of (b) 3.54, (c) 6.63, (d) 7.96, and (e) 8.84 J/cm^2. The yellow arrows indicate the direction of light polarization.

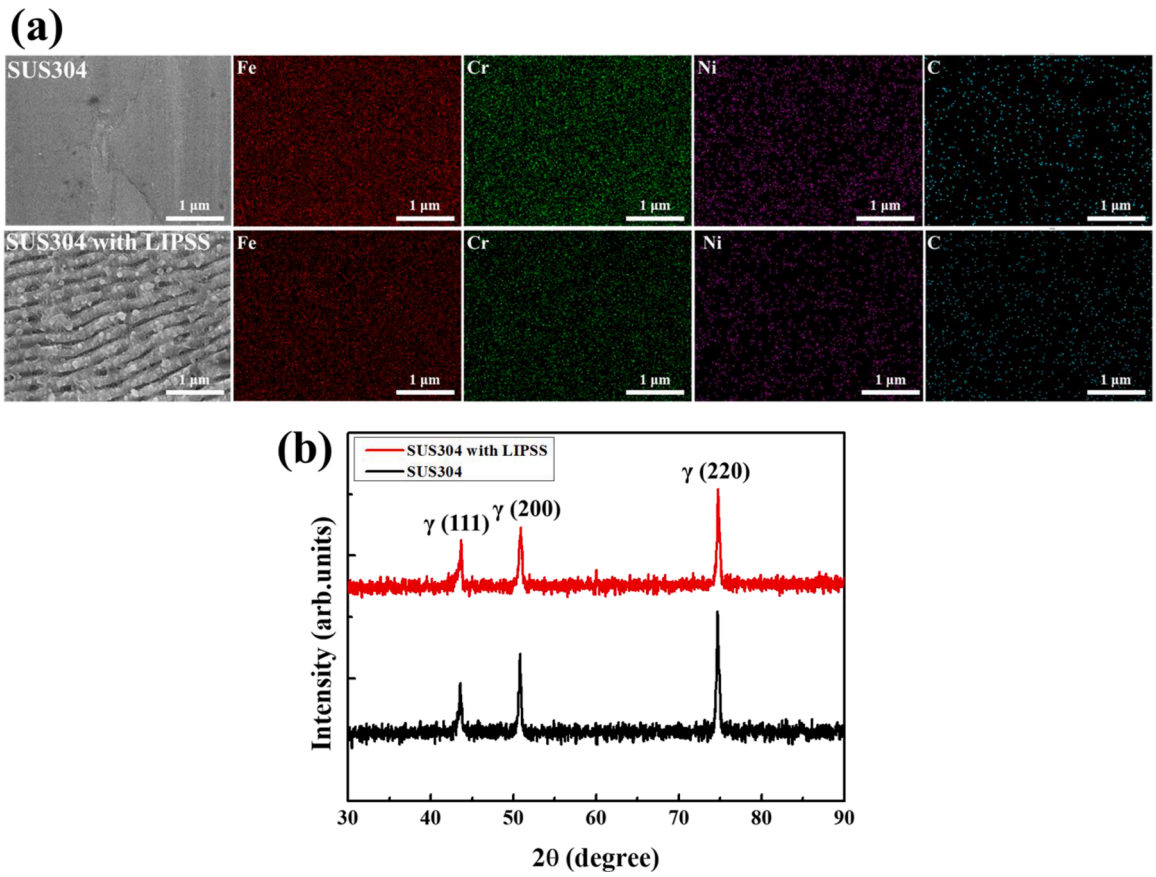

Fig. 2. (a) EDS mapping results and (b) XRD patterns of polished SUS304 surface and SUS304 surfaces with LIPSSs.

Table 1
Elemental compositions of unirradiated and picosecond laser-irradiated SUS304 disks.

Element	SUS304 (Wt %)	SUS304 with LIPSS (Wt %)
Fe	70.11	69.71
Cr	17.94	18.51
Ni	9.04	9.08
Si	1.03	0.95
Mn	1.86	1.77
Total:	100.00	100.00

topographies with micro/nano-dimples on the laser-textured surface [30].

3.3. Plate assays and bacterial growth curves on SUS304 and LIPSS specimens with Ag and Cu coatings

Table 2 presents the plate assay results for the antibacterial efficiencies of the SUS304 and SUS304+LIPSS samples, with and without Ag and Cu thin-film coatings. The uncoated SUS304 sample shows a large number of bacteria of each type. By contrast, the SUS304 and SUS304+LIPSS samples with Ag and Cu coatings show a 100 % antibacterial efficiency after contact for 24 h. Fig. 5(a), (b), and (c) show the bacterial growth curves of *E.coli, S.aureus,* and *P.aeruginosa* on the coated and uncoated substrates over the incubation period of 8 h. The OD values for the three bacterial strains in contact with the uncoated SUS304 sample increase sharply after 2 h. However, the bacterial strains in contact with the coated substrates (with or without LIPSSs) maintain low and constant OD values throughout the incubation period. Thus, it appears that the coatings damage the cell structures of the bacteria, which prevents their normal proliferation. The Ag and Cu coatings exhibit similar inhibitory effects, showing that both coatings have the potential to suppress bacterial growth. The contact angles (CAs) of the SUS304 samples with LIPSSs are higher than those of the non-irradiated SUS304 (Fig. 4). However, the results presented in Fig. 5 and Table 2 show no significant differences in the antibacterial efficacies of the different samples. Thus, it is inferred that the surface properties the irradiated samples have little or no effect on their antibacterial performance.

3.4. Accumulation of ROS and viability of bacteria on SUS304 and LIPSS specimens with Ag and Cu films

The accumulation of Reactive oxygen species (ROS) on the SUS304 and SUS304+LIPSS surfaces seeded with *E.coli, S.aureus,* and *P.aeruginosa* was examined using H_2DCFDA fluorescent probe. Fig. 6(a) presents the fluorescence images for the various treatments, where the green fluorescence indicates ROS accumulation. For all three bacterial strains, no ROS accumulation is observed on the uncoated SUS304 sample. However, substantial ROS accumulation occurs on the SUS304 samples with Ag and Cu coatings, both with and without LIPSSs. Fig. 6(b) shows the quantified ROS accumulation results for the various specimens. The samples with Ag coatings exhibit greater ROS accumulation than those with Cu coatings. Furthermore, the SUS304+LIPSSs samples with Ag and Cu coatings have higher ROS accumulation than the non-irradiated SUS304 samples with the same coatings. ROS have high toxicity toward microorganisms and cause cell rupture and death [31,32]. Specifically, ROS (especially H_2O_2) disrupts the cell membranes and interferes with DNA replication by damaging the purines and pyrimidines [31,33]. Furthermore, the metal ions of ROS depolarize the mitochondrial membrane and disrupt the electron transport chain by activating NADPH-related enzymes [33,34]. This further compromises the cell membranes and affects their metabolism and DNA replication.

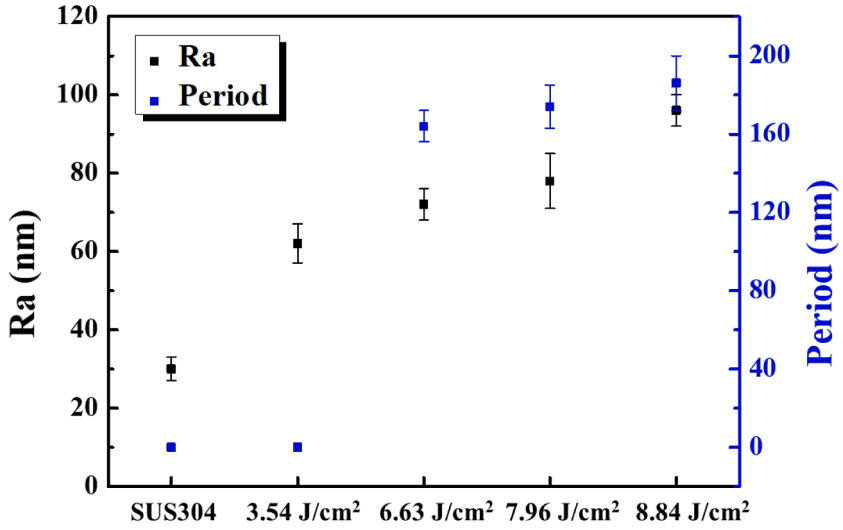

Fig. 3. Relationships between surface roughness (Ra), laser fluence, and LIPSS period for SUS304 samples processed by picosecond laser. The error bars indicate the standard error calculated from three replicate experiments.

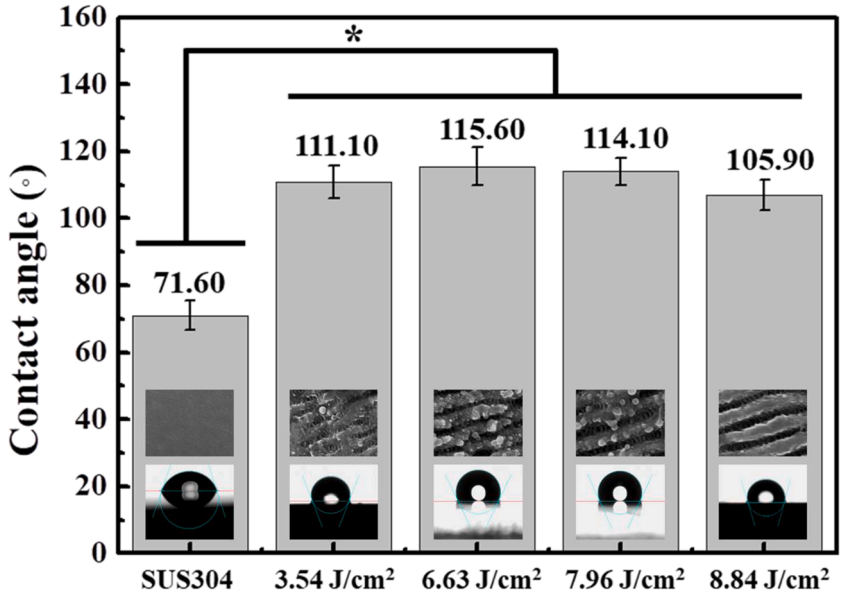

Fig. 4. Water droplet contact angles on SUS304 surface and SUS304 surfaces with LIPSSs produced using fluences of 3.54, 6.63, 7.96, and 8.84 J/cm^2 (*$p < 0.05$). The error bars show the standard error via three measurements.

Table 2
Antibacterial efficacy of SUS304 and SUS304 surfaces with LIPSSs and 15 nm-thick Ag and Cu coatings for *E. coli, S. aureus*, and *P. aeruginosa* based on CFU counts after 8 h of incubation. Antibacterial efficacy is evaluated as AE (%) = $[(A - B)/A] \times 100$, where A is the CFU value for SUS304 and B is the CFU value for SUS304 or SUS304 with LIPSS and Ag or Cu films.

Treatments	*E. coli*	*S. aureus*	*P. aeruginosa*
SUS304 (CK)	3.42×10^8	5.68×10^8	4.89×10^8
SUS304+Ag film	0 (100 %)	0 (100 %)	0 (100 %)
SUS304 with LIPSS+Ag film	0 (100 %)	0 (100 %)	0 (100 %)
SUS304+Cu film	0 (100 %)	0 (100 %)	0 (100 %)
SUS304 with LIPSS+Cu film	0 (100 %)	0 (100 %)	0 (100 %)

Moreover, ROS can also react with phospholipids, carbohydrates, amino acids, and nucleic acids [35] to cause bacterial death. The release of ROS from the present Ag and Cu coatings leads to elevated ROS levels in the *E. coli, S. aureus,* and *P. aeruginosa* cells, which damages their membranes and causes leakage of the intracellular protein, ultimately resulting in their death.

The viability of the bacterial strains on the SUS304 and SUS304-+LIPSS samples with Ag and Cu coatings was evaluated using the PI staining method. Fig. 7(a) shows the corresponding fluorescence images. For all three strains, the uncoated SUS304 sample shows a large quantity of green fluorescence (live cells) but relatively little red fluorescence (dead cells). In contrast, the SUS304 and SUS304+LIPSS samples with Ag and Cu coatings show a small amount of green fluorescence but a large amount of red fluorescence. Fig. 7(b) shows the ImageJ quantification results for the live and dead cells on the various samples. It can be seen that all the coated samples suppress bacterial growth and induce cell death. In addition, the laser-irradiated samples with LIPSSs and Ag and Cu coatings show a greater proportion of dead cells than the non-irradiated samples without LIPSS. Overall, the ROS and viability results indicate that the coating material (Ag or Cu) and the presence (or otherwise) of nanostructures play key roles in determining the ROS

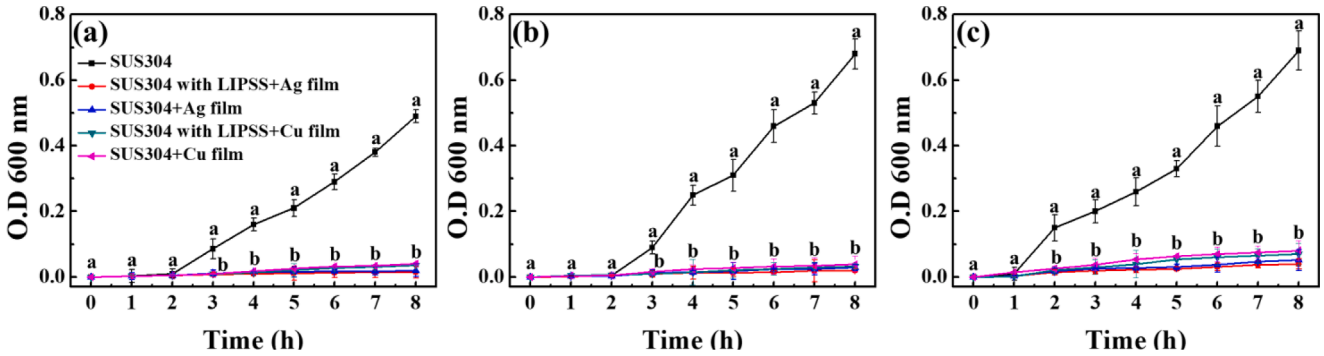

Fig. 5. Bacterial growth curves of (a) *E. coli*, (b) *S. aureus*, and (c) *P. aeruginosa* in contact with SUS304 and SUS304 surfaces with LIPSSs and 15 nm-thick Ag and Cu thin films. The different letters indicate significant differences according to Tukey's HSD test ($P < 0.05$).

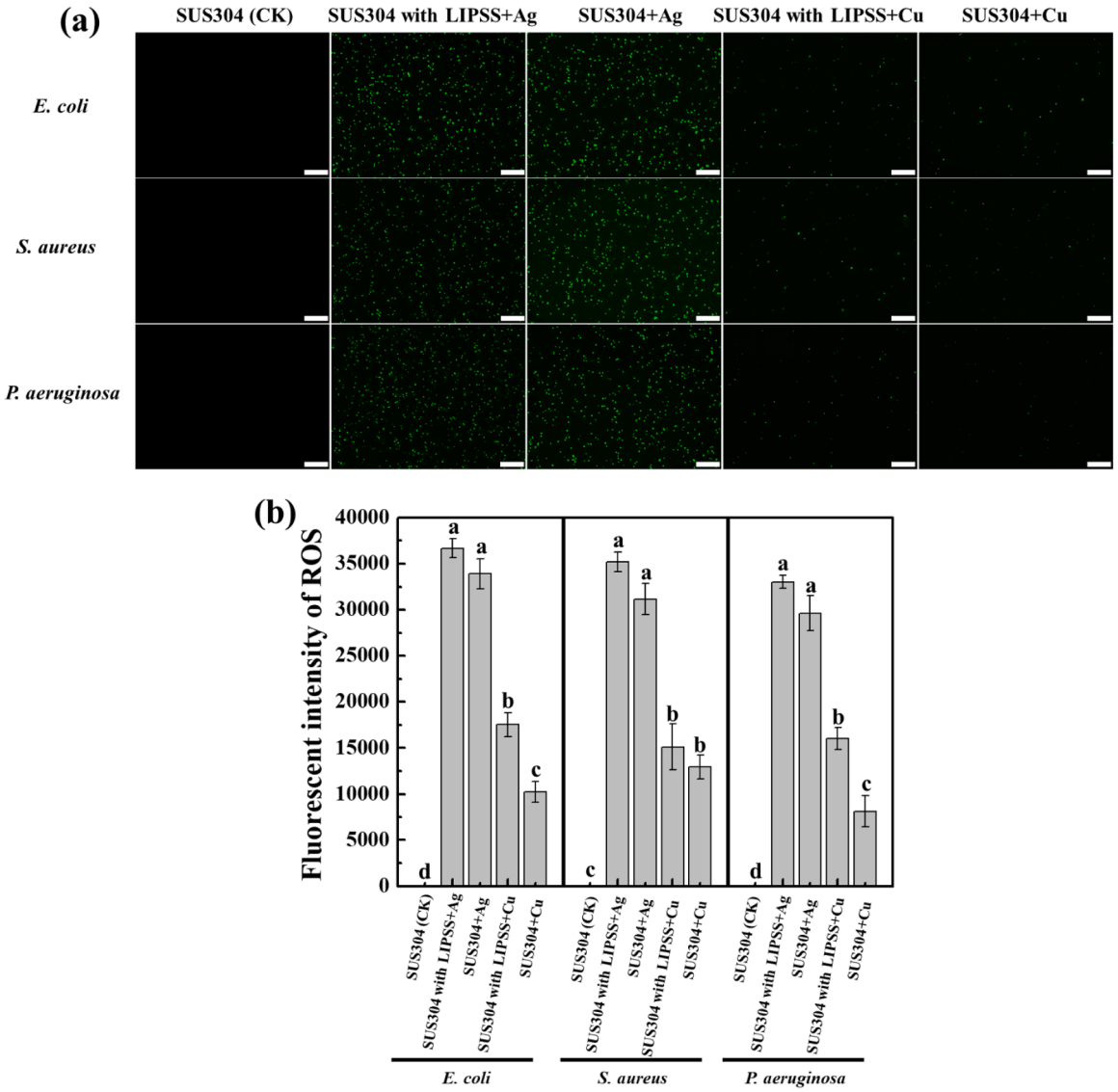

Fig. 6. Effects of SUS304 and SUS304 surfaces with LIPSSs and 15 nm-thick Ag and Cu thin coatings on ROS generation for *E. coli, S. aureus*, and *P. aeruginosa* after contact for 24 h. (a) ROS generation. Scale bars indicate length of 20 μm. (b) Fluorescence intensity of ROS as determined using ImageJ software. The different letters indicate significant differences according to Tukey's HSD test ($P < 0.05$).

accumulation and antibacterial properties of the SUS304 surface. Together with ROS accumulation data, these results indicate that both the coating material (Ag or Cu) and the presence of surface nanostructures significantly influence the antibacterial performance of the SUS304 substrates. Based on the observed ROS accumulation and bacterial viability results, it is inferred that Ag and Cu coatings has their

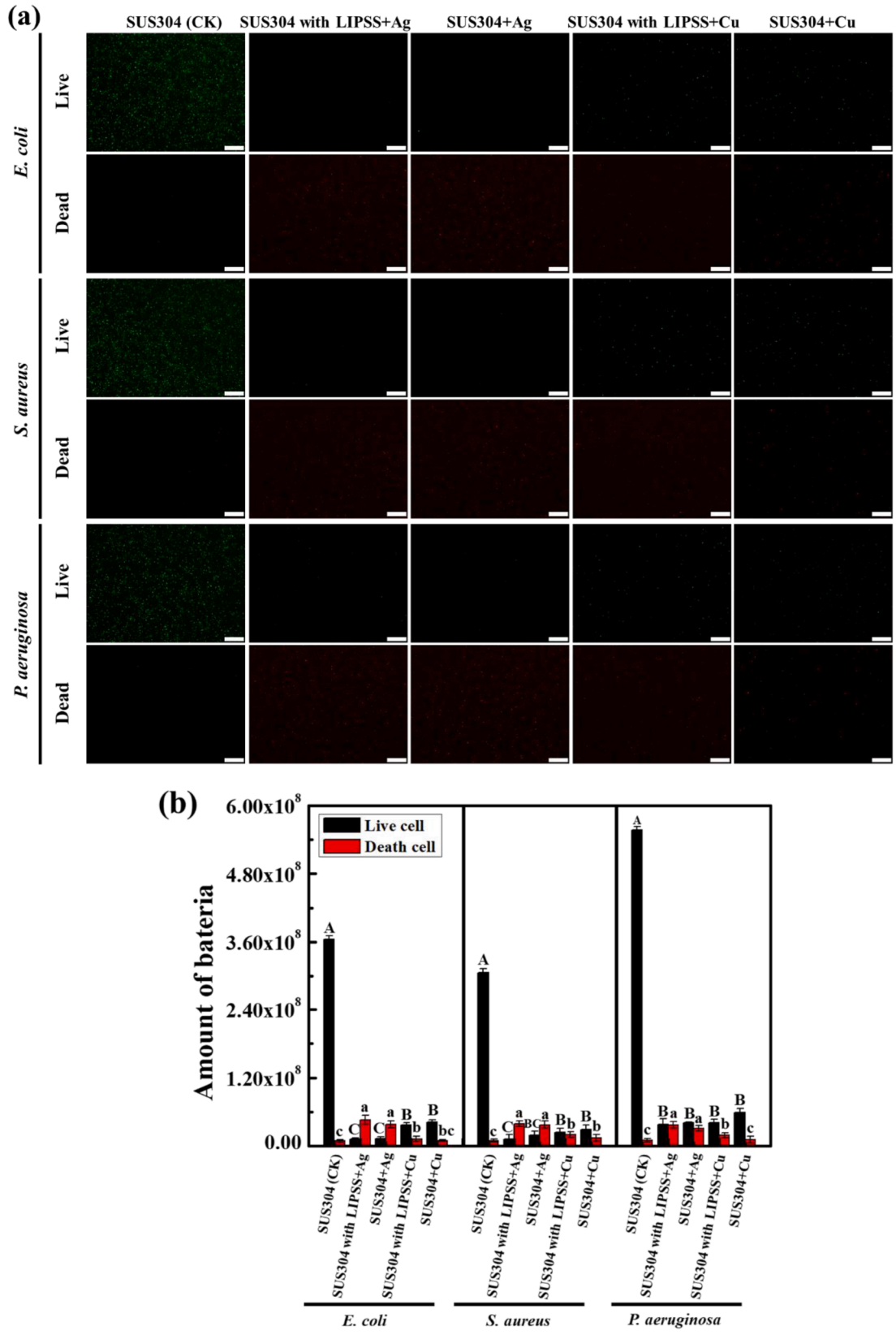

Fig.. 7. Viability of *E. coli, S. aureus*, and *P. aeruginosa* following contact with SUS304 and SUS304 surfaces with LIPSSs and 15 nm-thick Ag and Cu thin films for 24 h. (a) Live/dead cells. Green fluorescence indicates live bacteria; red fluorescence shows dead bacteria. Scale bars indicate length of 20 μm. (b) Live/dead cell counts for *E. coli*, S. aureus, and P. aeruginosa after 24 hrs. Capital letters indicate statistical comparisons for live cell data, while lowercase letters indicate those for dead cell data. The different letters indicate significant differences according to Tukey's HSD test ($P < 0.05$).

antibacterial effects through different mechanisms. silver has been extensively reported to induce the generation of ROS, which contributes to oxidative damage of bacterial membranes and intracellular component [36]. In contrast, copper has antibacterial effect through multiple ROS-independent mechanisms. The study [37] indicated that copper nanoparticles disrupt membrane potential in *E. coli*, leading to filamentation and intracellular content leakage. They also reported oxidative damage to lipids, proteins, and DNA, with DNA degradation significantly reduced by EDTA, indicating a key role of Cu^{2+} ions. These findings suggest that the antibacterial activity of copper is largely driven by ion release and direct membrane interaction, rather than ROS accumulation alone.

The cell proliferation of the *E.coli, S.aureus,* and *P.aeruginosa* strains on the coated SUS304 and SUS304+LIPSS samples was further evaluated using alamarBlue assays. As shown in Fig. 8, the original SUS304 sample without LIPSSs or metal coatings showed a very high cell proliferation rate. However, all the metal-coated samples demonstrated a very low cell activity, irrespective of the presence (or otherwise) of LIPSSs. Among all the samples, the SUS304+LIPSS sample coated with an Ag film showed the lowest cell proliferation for all three bacterial strains.

4. Conclusions

SUS304 disks were processed using a picosecond UV laser with various laser fluences to induce periodic surface structures (LIPSSs). Ag and Cu coatings with thicknesses of 15 nm were deposited on the non-irradiated and irradiated samples using a sputtering system. The morphologies, crystal structures, and elemental segregations of the various samples were examined and compared. The antibacterial effects of the coated and uncoated specimens against *E. coli, S. aureus,* and *P. aeruginosa* were also explored.

The results showed that the surface roughness (Ra), ripple period (Λ), and contact angle (CA) increased with an increasing laser fluence. However, no element segregation or phase transition was observed following laser treatment. The SUS304 and SUS304+LIPSS samples with Ag and Cu coatings showed an excellent antibacterial effect against *E. coli, S. aureus,* and *P. aeruginosa* after 24 h of contact due to the accumulation of ROS and release of metal ions from the coating. Of all the samples, the SUS304+LIPSS sample with the Ag coating showed the highest accumulation of ROS and the greatest cytotoxicity. Overall, the results confirm the feasibility of picosecond UV laser treatment for the surface nano-texturing of SUS304 for biomaterial applications.

Author contributions

J. J. Wang participated in the design of the thin film and helped to draft the manuscript. PhD student Y.Z. Xu carried out plate assays and bacterial experiments. C.M. Chen carried out the laser studies. Y.C. Lin and Dr. C.J. Huang did some laser experiments. Prof. Y.H. Lin participated in the design of bacterial experiments. Prof. Lin conceived of the study, participated in its design and drafted the manuscript. All authors discussed the results and commented on the manuscript. All authors read and approved the final manuscript.

CRediT authorship contribution statement

Jyun-Jhih Wang: Writing – original draft, Investigation, Data curation, Conceptualization. **Ya-Zhen Xu:** Methodology, Investigation, Data curation. **Chun-Ming Chen:** Investigation, Formal analysis, Data curation. **Yu-Chung Lin:** Methodology, Investigation. **Chien-Jung Huang:** Visualization, Methodology, Formal analysis. **Ying-Hong Lin:** Supervision, Resources, Investigation. **Hsuan-Kai Lin:** Writing – review & editing, Writing – original draft, Supervision, Resources, Investigation, Funding acquisition, Conceptualization.

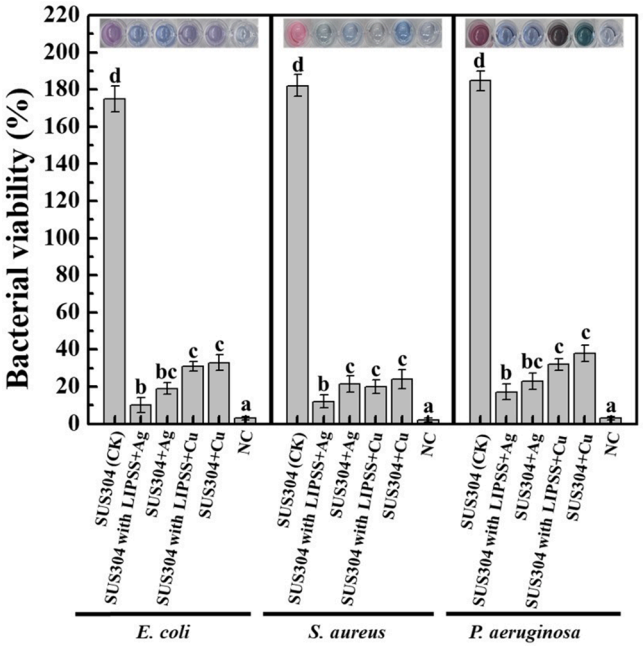

Fig. 8. AlarmarBlue assay on *E. coli, S. aureus*, and *P. aeruginosa* following contact with SUS304 and SUS304 surfaces with LIPSSs and 15 nm-thick Ag and Cu thin films for 24 h. NC indicates negative control. The different letters indicate significant differences according to Tukey's HSD test ($P < 0.05$).

Declaration of competing interest

The authors declare that they have no known competing financial interests or personal relationships that could have appeared to influence the work reported in this paper.

Acknowledgements

The authors gratefully acknowledge the financial support provided to this study by the National Science and Technology Council, ROC, under project no NSTC 112-2637-E-020-004.

Data availability

Data will be made available on request.

References

[1] A. Sikora, M. Faucon, L. Gemini, R. Kling, G. Mincuzzi, LIPSS and DLIP: from hierarchical to mutually interacting, homogeneous, structuring, Appl. Surf. Sci. 591 (2022).
[2] E. Fadeeva, B. Chichkov, Biomimetic liquid-repellent surfaces by ultrafast laser processing, Appl. Sci. 8 (9) (2018).
[3] J. Bonse, S.V. Kirner, M. Griepentrog, D. Spaltmann, J. Kruger, Femtosecond laser texturing of surfaces for tribological applications, Mater. (Basel) 11 (5) (2018).
[4] P. Bizi-bandoki, S. Valette, E. Audouard, S. Benayoun, Time dependency of the hydrophilicity and hydrophobicity of metallic alloys subjected to femtosecond laser irradiations, Appl. Surf. Sci. 273 (2013) 399–407.
[5] A. Ruiz de la Cruz, R. Lahoz, J. Siegel, G.F. de la Fuente, J. Solis, High speed inscription of uniform, large-area laser-induced periodic surface structures in Cr films using a high repetition rate fs laser, Opt. Lett. 39 (8) (2014) 2491–2494.
[6] I. Gnilitskyi, T.J. Derrien, Y. Levy, N.M. Bulgakova, T. Mocek, L. Orazi, High-speed manufacturing of highly regular femtosecond laser-induced periodic surface structures: physical origin of regularity, Sci. Rep. 7 (1) (2017) 8485.
[7] A.Y. Vorobyev, V.S. Makin, C. Guo, Brighter light sources from black metal: significant increase in emission efficiency of incandescent light sources, Phys. Rev. Lett. 102 (23) (2009) 234301.
[8] N. Tagawa, M. Takada, A. Mori, H. Sawada, K. Kawahara, Development of contact sliders with nanotextures by femtosecond laser processing, Tribol. Lett. 24 (2) (2006) 143–149.
[9] A. Papadopoulos, E. Skoulas, A. Mimidis, G. Perrakis, G. Kenanakis, G.D. Tsibidis, E. Stratakis, Biomimetic omnidirectional antireflective glass via direct ultrafast laser nanostructuring, Adv. Mater. 31 (32) (2019) e1901123.

[10] C. Richards, A. Slaimi, N.E. O'Connor, A. Barrett, S. Kwiatkowska, F. Regan, Bio-inspired surface texture modification as a viable feature of future aquatic antifouling strategies: a review, Int. J. Mol. Sci. 21 (14) (2020).
[11] L. Dou, L. Yang, S. Wang, B. Zhang, W. Zhu, Y. Jiang, Z. Yu, Q. Wu, Dry friction and wear behavior of volcano arrays based mixed morphology textured by femtosecond laser, Mater. Today Commun. 34 (2023).
[12] S. Song, Q. Lu, P. Zhang, H. Yan, H. Shi, Z. Yu, T. Sun, Z. Luo, Y. Tian, A critical review on the simulation of ultra-short pulse laser-metal interactions based on a two-temperature model (TTM), Opt. Laser Technol. 159 (2023) 109001.
[13] J. Bonse, S. Höhm, S.V. Kirner, A. Rosenfeld, J. Krüger, Laser-induced periodic surface structures— a scientific evergreen, IEEE J. Select. Top. Quant. Electron. 23 (3) (2017) 1.
[14] Y.-H. Lin, J.-J. Wang, Y.-T. Wang, H.-K. Lin, Y.-J. Lin, Antifungal properties of pure silver films with nanoparticles induced by pulsed-laser dewetting process, Appl. Sci. 10 (7) (2020).
[15] Y.Y. Chu, Y.S. Lin, C.M. Chang, J.K. Liu, C.H. Chen, J.C. Huang, Promising antimicrobial capability of thin film metallic glasses, Mater. Sci. Eng. C Mater. Biol. Appl. 36 (2014) 221–225.
[16] J.-J. Wang, I.C. Chen, H.-K. Lin, Y.-C. Lin, C.-J. Huang, Preparation of uniform Ag nanoparticles with enhanced plasmon resonance intensity and antibacterial efficiency via two-step dewetting process, Opt. Laser Technol. 168 (2024).
[17] J.J. Wang, H.K. Lin, W.S. Chuang, C.Y. Chuang, Y.-H. Lin, J.C. Huang, Y.-H. Lin, Laser dewetting mechanism and antibacterial properties of Cu-Al based medium entropy alloy films, J. Alloy. Compd. 903 (2022).
[18] M. Okazaki, M. Hashida, S. Iwamori, Antibacterial effect of periodic structure formed on SUS430 by using nanosecond pulsed laser, J. Laser Appl. 35 (4) (2023).
[19] E. Agbangba, E. Sacla Aide, S.H. Honfo, R.L. Glele Kakaï, On the use of post-hoc tests in environmental and biological sciences: a critical review, Heliyon 10 (2024) e25131.
[20] J.W. Tukey, Comparing individual means in the analysis of variance, Biometrics 5 (2) (1949) 99–114.
[21] A. San-Blas, M. Martinez-Calderon, E. Granados, M. Gómez-Aranzadi, A. Rodríguez, S.M. Olaizola, LIPSS manufacturing with regularity control through laser wavefront curvature, Surface. Interface. 25 (2021).
[22] J. Bonse, Quo Vadis LIPSS?-Recent and Future Trends on Laser-Induced Periodic Surface Structures, Nanomater. (Basel) 10 (10) (2020).
[23] Z. He, Y. Shen, J. Tao, H. Chen, X. Zeng, X. Huang, A.A. El-Aty, Laser shock peening regulating aluminum alloy surface residual stresses for enhancing the mechanical properties: roles of shock number and energy, Surface Coat. Technol. 421 (2021).
[24] Q. Zhang, Y. Guan, Laser induced periodic surface structure on titanium alloy and its effect on microstructure refinement and corrosion behavior, J. Alloy. Compd. 936 (2023).
[25] J. Outón, T. Córdoba, E. Gallero, M. Vlahou, E. Stratakis, V. Matres, E. Blanco, Corrosion behavior of nanostructured ferritic stainless steel by the generation of LIPSS with ultrashort laser pulses, J. Mater. Res. Technol. 27 (2023) 7422–7433.
[26] U. Hermens, S.V. Kirner, C. Emonts, P. Comanns, E. Skoulas, A. Mimidis, H. Mescheder, K. Winands, J. Krüger, E. Stratakis, J. Bonse, Mimicking lizard-like surface structures upon ultrashort laser pulse irradiation of inorganic materials, Appl. Surf. Sci. 418 (2017) 499–507.
[27] L. Petan, J.L. Ocaña, J. Grum, Influence of laser shock peening pulse density and spot size on the surface integrity of X2NiCoMo18-9-5 maraging steel, Surface Coat. Technol. 307 (2016) 262–270.
[28] A. Daneshnia, K. Raeissi, P. Salehikahrizsangi, Rapid one-step electrodeposition of robust superhydrophobic and oleophobic Ni coating with anti-corrosion and self-cleaning properties, Surface Coat. Technol. 450 (2022).
[29] J. Meng, Y. Xie, Y.-H. Gu, X. Yan, Y. Chen, X.-J. Guo, W.-Z. Lang, PVDF-CaAlg nanofiltration membranes with dual thin-film-composite (TFC) structure and high permeation flux for dye removal, Sep. Purif. Technol. 255 (2021).
[30] X. Sedao, M. Lenci, A. Rudenko, N. Faure, A. Pascale-Hamri, J.P. Colombier, C. Mauclair, Influence of pulse repetition rate on morphology and material removal rate of ultrafast laser ablated metallic surfaces, Opt. Laser. Eng. 116 (2019) 68–74.
[31] S.J. Soenen, P. Rivera-Gil, J.-M. Montenegro, W.J. Parak, S.C. De Smedt, K. Braeckmans, Cellular toxicity of inorganic nanoparticles: common aspects and guidelines for improved nanotoxicity evaluation, Nano Today 6 (5) (2011) 446–465.
[32] P.V. AshaRani, G. Low Kah Mun, M.P. Hande, S. Valiyaveettil, Cytotoxicity and genotoxicity of silver nanoparticles in human cells, ACS Nano 3 (2) (2009), 279–90.
[33] X. Huang, D. He, Z. Pan, G. Luo, J. Deng, Reactive-oxygen-species-scavenging nanomaterials for resolving inflammation, Mater. Today Bio. 11 (2021) 100124.
[34] K.R. Smith, L.R. Klei, A. Barchowsky, Arsenite stimulates plasma membrane NADPH oxidase in vascular endothelial cells, Am. J. Physiol. Lung Cell Mol. Physiol. 280 (3) (2001) L442–L449.
[35] Q. Xu, C. He, C. Xiao, X. Chen, Reactive oxygen species (ROS) responsive polymers for biomedical applications, Macromol. Biosci. 16 (5) (2016) 635–646.
[36] Y.N. Slavin, J. Asnis, U.O. Häfeli, H. Bach, Metal nanoparticles: understanding the mechanisms behind antibacterial activity, J. Nanobiotechnol. 15 (1) (2017) 65.
[37] A.K. Chatterjee, R. Chakraborty, T. Basu, Mechanism of antibacterial activity of copper nanoparticles, Nanotechnology 25 (13) (2014) 135101.